Airborne measurements of atmospheric methane column abundance made using a pulsed IPDA lidar

Haris Riris,[1*], Kenji Numata,[2] Steve Li,[3] Stewart Wu,[3] Anand Ramanathan,[1] Martha Dawsey,[1] Jianping Mao,[4] Randolph Kawa,[1] and James B. Abshire[1]

[1]NASA- Goddard Space Flight Center, Science and Exploration Directorate, Greenbelt, MD 20771, USA
[2]Department of Astronomy, University of Maryland, College Park, MD 20742, USA
[3]NASA- Goddard Space Flight Center, Lasers and Electro-Optics Branch, Greenbelt, MD 20771, USA
[4]Goddard Earth Sciences Technology and Research, Goddard Space Flight Center, 8800 Greenbelt, Rd, Greenbelt, MD, 20771, USA

[*]Corresponding author: haris.riris@nasa.gov

Abstract: We report airborne measurements of the column abundance of atmospheric methane made over an altitude range of 3-11 km using a direct detection IPDA lidar with a pulsed laser emitting at 1651 nm. The laser transmitter was a tunable, seeded optical parametric amplifier (OPA) pumped by a Nd:YAG laser and the receiver used a photomultiplier detector and photon counting electronics. The results follow the expected changes with aircraft altitude and the measured line shapes and optical depths show good agreement with theoretical calculations.

OCIS codes: 010.0280, 280.1910, 280.3640, 300.1030.

1. Introduction

The last report by the Intergovernmental Panel on Climate Change [**Error! Reference source not found.**] attributes the increase of the atmospheric concentrations of greenhouse gases above their pre-industrial levels to the burning of fossil fuels and other anthropogenic sources. As the concentration of greenhouse gases steadily increases the subsequent radiative forcing will likely have a significant impact on Earth's climate. Presently our knowledge and understanding of the important processes controlling greenhouse gas concentrations is incomplete. Current observations of greenhouse gases are mostly from in-situ (surface and tower) sites, airborne, and space-based measurements from passive spectrometers. Initial space measurements of methane and other greenhouse gases came from SCIAMACHY on ESA's ENVISAT mission [2-4], the Infrared Atmospheric Sounding Interferometer (IASI) on CNES' MetOp satellite [5,6], and NASA's Atmospheric Infrared Sounder (AIRS) on NASA's Aqua Mission [7,8]. Additional space measurements are now available from JAXA's GOSAT mission, which was launched in 2009 [9-12]. All four instruments are passive spectrometers and their observations are limited. Measurements using surface reflected sunlight by GOSAT and SCIAMACHY are limited to the sunlit areas of earth and their data products are significantly affected by atmospheric scattering and the presence of clouds [13, 14]; measurements in thermal infrared by AIRS and IASI have measurement weighting function peaked in the mid-troposphere [15] and are not sensitive to the sources and sinks of greenhouse gases at the surface but are very sensitive to atmospheric temperature changes.

Although CO_2 is currently the largest carbon-based greenhouse gas, methane is also important since its radiative forcing is approximately 23 times larger per molecule than CO_2 [**Error! Reference source not found.**]. The methane mixing ratio is presently at ~1.8 parts per million by volume (ppmv) and has been increasing along with CO_2 [**Error! Reference source not found.**6, 17]. Natural sources of methane include wetlands, wild fires, and termites [15]. Anthropogenic sources of methane include fossil fuel production, rice farming, livestock and landfills. Important sinks for methane include oxidation by hydroxyl radicals in the atmosphere and oxidation by non-saturated soils.

Large amounts of methane are also contained in the continental shelf in the form of methane hydrates [18]. The large reservoirs of carbon trapped in the permafrost regions of northern North America, Europe, and Siberia are a major concern. As global temperatures rise and the permafrost thaws, some of the carbon will be converted to methane and will be released into the atmosphere adversely affecting the climate [19-20]. Better knowledge of the methane distribution and understanding of the sources and sinks is imperative for a better assessment of its impact on global change [21-23].

The US National Research Council also recognized the importance of measuring methane and in its last Decadal Survey for Earth Science [24], which recommended that NASA implement an active (laser) based space mission to measure CO_2 emissions called ASCENDS and added the following statement: "*Ideally, to close the carbon budget, methane should also be addressed, but the required technology is not now obvious. If appropriate and cost-effective methane technology becomes available, methane capability should be added*". The ASCENDS working group is in the process of defining measurement requirements for the mission [25]. Although the final ASCENDS requirements have not yet been released, its launch date has been deferred by budgetary constraints.

The French Centre National d'Etudes Spatiales (CNES) in collaboration with the German Aerospace Centre (DLR) are developing a small lidar-based methane mission called MERLIN (Methane Remote Sensing Lidar Mission) scheduled for launch in 2016 [26-28]. The MERLIN mission targets an 8 ppbv relative random error in the methane column abundance with a 50 km horizontal resolution to be scientifically useful.

Measuring methane and its isotopes in planetary atmospheres can aid in understanding planetary processes and in the search for extraterrestrial life. Habitable environments are believed to have existed previously on Mars and could potentially persist today. The presence and distribution of methane and other gases of possible biogenic origin may provide evidence for subsurface biology and help better locate regions for more intensive study. Recent planetary missions and ground-based observations have provided evidence of reservoirs of methane and water on Mars [29-33] that could potentially harbor life. The observations also suggested large seasonal and spatial variations of methane concentrations.

The Mars Trace Gas Orbiter (TGO) is an ESA mission currently under development that is scheduled to launch in 2016 [34]. It will make very sensitive measurements of a broad suite of atmospheric trace gases, and characterize the spatial and temporal variability of methane and other key species with passive spectrometers. In the future, a laser-based spectrometer (a lidar) can provide much better spatial resolution to localize areas of high methane concentrations (e.g. plumes or vents) discovered by TGO and map the global distribution of these gases over day and night and at all latitudes. The requirements for an active methane instrument on Mars are likely to require 1 ppb (or below) detection sensitivity over a relatively small area (a few tens of km^2) in order to localize methane sources. For these applications, measuring methane is a detection problem – i.e. detecting the presence of a small signal against a small background.

At Goddard Space Flight Center (GSFC) we have developed lidar technology based on Optical Parametric Amplifiers (OPA) that can be used to measure methane remotely from an orbiting platform. The transmitter technology is applicable to both Earth and planetary atmospheres but requires different detectors. Using this technology we have demonstrated measurements of methane, carbon monoxide and dioxide, and water vapor on the ground [35,36] and in the summer of 2011 we demonstrated methane measurements from an airborne platform in California at altitudes from 3 to 11 km. The latter measurements are the subject of this work.

2. Methane Spectroscopy

Methane has absorptions in most of the near and mid-IR spectral range. The strongest bands are at 1.65, 2.2, 3.3, and 7.8 μm. The band at 3.3 μm is ideal for making high sensitivity measurements of methane in low-pressure planetary atmospheres, such as Mars. The average surface pressure on Mars is ~ 6 mbar, which results in negligible pressure broadening (typically less than < 30 MHz full-width-half-maximum) so the absorption lines are essentially Doppler-broadened. A laser spectrometer with sufficient signal to noise ratio (SNR) and high spectral resolution would be an ideal candidate for measuring methane from a Mars orbit.

In the Earth's atmosphere the methane lines in the 3.3 μm spectral region may be suitable for pipeline leak detection and other similar low altitude applications [37-40] that use relatively short paths (typically <1 km) and for in-situ detection [41-43]. However, most methane lines near 3.3 μm are too strong for space use since they would completely absorb the laser radiation before it reaches the ground. There is also significant interference from the wings of adjacent water vapor and other absorption lines in this spectral region. Water vapor is a particular issue

since it is highly variable in the Earth's atmosphere, and would make accurate measurements of methane from space at 3.3 μm very difficult.

The overtones lines methane at 1.65 μm, however, are well suited for remote sensing of atmospheric methane in the Earth's atmosphere. The lines are almost two orders of magnitude weaker than those at 3.3 μm, but they are relatively free of interference from other atmospheric species. For example, Figure 1 shows the two-way transmittance through a US standard atmosphere from an orbit of 400 km for a methane line at 1650.95 nm calculated using the HITRAN 2008 database [44]. This candidate methane line is strong enough to be used for lidar observations and has very little interference from other species.

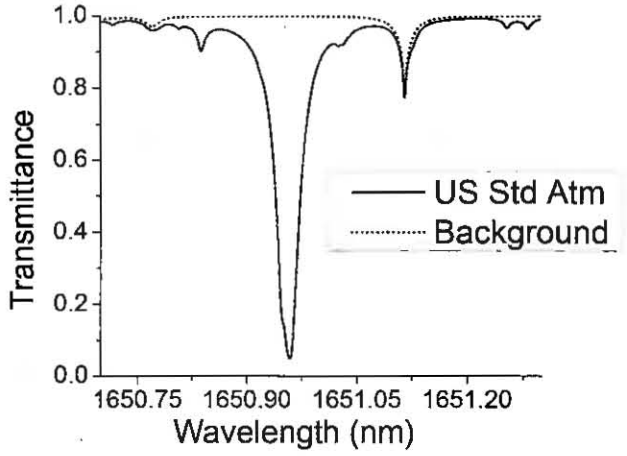

Figure 1 Two-way atmospheric transmittance of methane at 1651 nm from a 400 km orbit for a US standard atmosphere. The dotted curve is the two-way atmospheric transmittance without methane (background).

3. Laser approach and technology

We have developed a direct detection lidar to measure column methane abundance using the integrated path differential absorption (IPDA) technique. It uses a tunable pulsed laser whose spectral emission can be rapidly tuned across a selected methane absorption line, and a time resolved receiver using a sensitive detector to detect the reflected laser energy.

We chose a laser based on Optical Parametric Generation (OPG) to generate tunable radiation at 1.65 and 3.3 μm. In OPG, a photon of an incident laser pulse (pump) is divided into two photons, a signal and an idler, by a nonlinear optical crystal. The wavelengths of the signal and the idler must that satisfy the energy and phase matching conditions in the crystal. An Optical Parametric Amplifier (OPA) is a seeded version of OPG.

A simplified block diagram of our OPA-based lidar is shown in Figure 2. A nonlinear periodically poled Lithium Niobate (PPLN) crystal is pumped by a pulsed single-frequency 1064 nm Nd:YAG laser and seeded by a continuous-wave (CW) 1651 nm distributed-feedback (DFB) laser diode. The wavelength of the seed laser can be easily changed by changing the diode laser. We used seed laser diodes at 1578 nm to generate an idler wavelength at 3.3 μm and 1651 nm to amplify the seed wavelength for 1651 nm applications. In principle, any diode laser between 1530 nm and 1660 nm can be used as a seed in order to target different trace gases in the 1.5-1.65 μm and 3-4 μm range. Diode lasers are small, rugged, and have very desirable spectroscopic characteristics: their side mode suppression ratio typically exceeds 40 dB, they tune smoothly over a few nm, their wavelength can be tightly controlled via the temperature and

current to the diode and the instantaneous linewidth can be less than 1 MHz. They also can also be frequency stabilized using external reference cells [45].

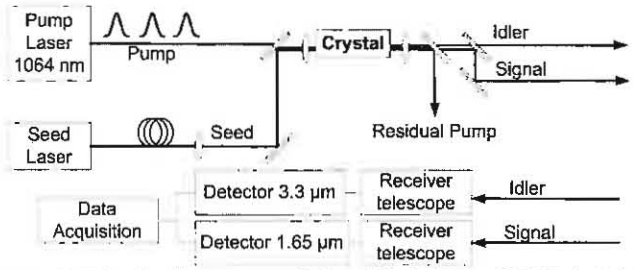

Figure 2 Block diagram of the OPA-based IPDA Lidar.

The two beams (seed and pump) are co-aligned and focused through the PPLN crystal. The temperature of the crystal can be tuned between 70 °C and 170 °C to optimize the phase matching at the target wavelength. The output beam is separated into three wavelength paths using dichroic mirrors. Depending on the application (Earth or Mars) the signal, the idler, or both can be used for trace gas detection through an absorption cell or in an open path. For open path measurements the returns at 1651 nm and 3.3 μm are collected by commercial telescopes and detected by InGaAs and HgCdZnTe detectors, respectively. The return signals are averaged by a boxcar averager and digitized by a computer for processing and display. A description of the different OPA systems we have used for ground-based measurements were given by Numata et.al. [35]. In this paper, we discuss using the OPA-based transmitter operating at 1651 nm to measure methane column abundance from an aircraft.

4. Airborne Lidar

For our airborne demonstration we used an enhancement of the IPDA technique [46], using a sequence of discrete laser pulses that were repetitively stepped in wavelength across the line. Ideally only two wavelengths are needed for an IPDA lidar to determine the line's transmission and determine the path integrated atmospheric column density. In practice, however, using more wavelengths and measuring the line shape is quite valuable. This additional data allows solving for variable instrumental and systematic errors, such as etalon fringes with various periods and baseline drifts. Our airborne methane lidar used 20 wavelengths distributed evenly across the line.

The methane lidar measures the total transmittance, $\tau(\nu)$, of the emitted laser energy E_o, through the atmospheric column (from the aircraft to the ground and back). The received energy, E, can be written as

$$E = E_0 \eta \frac{A}{R^2} \frac{\beta}{\pi} \tau^2(\nu) \qquad (1)$$

where, receiver efficiency, η, the ground surface reflectivity, β, the collecting area of the receiver, A, range to the surface, R, and ν is the laser frequency. The total transmittance over the atmospheric column is an integral over all atmospheric layers, dr, between the aircraft and the ground:

$$\tau(\nu) = e^{-2\int_0^R \sigma(\nu,T,P)N(r)dr} \quad (2)$$

where, $\sigma(\nu,T,P)$ is the molecular absorption cross section for a given atmospheric layer and $N(r)$ is the corresponding number density in each atmospheric layer.

The absorption cross section is a function of the temperature, T, and pressure, P, at each atmospheric layer and the natural logarithm of the transmittance, $ln(\tau(\nu))$, is usually referred to as the optical depth (OD). The differential optical depth (DOD), the OD "on" and "off" the absorption, at λ_{on} and λ_{off} is a useful quantity since, to first order, it increases linearly with the number density. As stated above, an IPDA lidar may be designed to use two wavelengths ("on" and "off" the absorption, λ_{on} and λ_{off}) or multiple wavelengths to trace the entire lineshape. The OD and DOD changes at λ_{on} and λ_{off} can be used to assess the signal to noise ratio (SNR) and performance of an IPDA lidar [47-50].

4.1 Laser Operation and Data Recorder

For airborne operations the ground-based methane instrument was modified to fit into the NASA DC-8. A more robust opto-mechanical design was implemented to prevent misalignment in the aircraft environment. A block diagram of the airborne instrument is shown in Figure 3. The pump laser is a passively Q-switched, Nd:YAG non-planar ring oscillator (NPRO) made by Innolight Inc. that emits single-frequency output at 1064.5 nm. It has 3 ns pulse width and maximum energy of 60 μJ per pulse at a 6.3 kHz repetition rate. The laser is operating in single mode and its optical linewidth is transform limited (~133 MHz). A beam splitter directs a small portion of the pump laser onto a high speed photodiode (EO Technologies ET-3000) that provides a trigger for the data acquisition sequence. The OPA is seeded by a CW 1651 nm commercial DFB laser made by NEL America (part no: NLK1U5FAAA). The two beams (pump and seed) are co-aligned and focused through the OPA crystal. The OPA crystal was a 50-mm long, 1-mm thick, MgO-doped PPLN with a 31.0 μm grating. The end surfaces of the crystal were angled at 5° and AR coated at the pump, the signal and the idler wavelengths, in order to minimize optical feedback and etalon fringes. The temperature of the crystal is controlled by an oven and temperature controller. The output beams from the OPA are collimated and separated into three wavelength paths using dichroic mirrors (not shown in Figure 3 for simplicity). The idler and residual pump wavelengths are not used in the airborne experiment. The signal beam from the OPA is sent through a beam expander to reduce its divergence to 250-300 μrad and then directed to the ground through the nadir port of the aircraft.

A beam splitter directs part of the outgoing 1651 nm beam through a short (8 cm) CH_4 reference cell containing 370 Torr that is used for wavelength calibration. Another part of the outgoing beam is sent on to an InGaAs detector (Thorlabs DET10C) that serves as an energy monitor. The output signal from the cell and the energy monitor are integrated by gated integrators (Signal Recovery Model 4121B) and then digitized by an analog to digital converter (ADC).

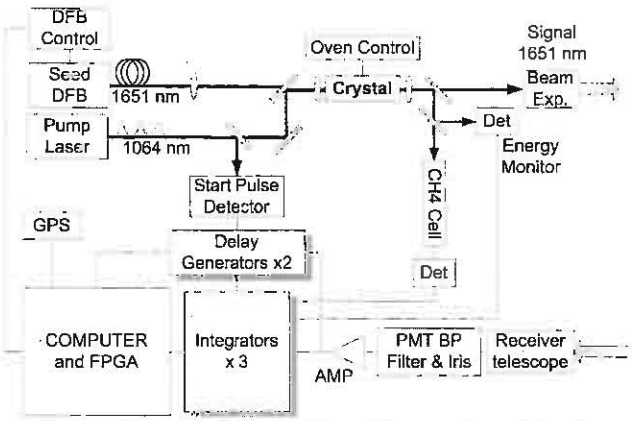

Figure 3. Block diagram of the airborne lidar. The idler and residual pump beams were not used and are not shown in the diagram.

The reflected ground echoes are collected by a commercial 20 cm diameter receiver telescope (Vixen VC200L) and are coupled into an AR coated 600-μm core multi-mode fiber (Fiberguide CB18167). The receiver field of view (FOV) is determined by the telescope effective focal length (2 m), the receiver fiber core size, and its numerical aperture (NA). In our case the FOV was 300 μrad. The receiver fiber output is collimated and directed through a 0.8 nm (FWHM) bandpass (BP) filter (Barr Associates), an iris for signal attenuation, and then onto a photon counting detector (Hamamatsu photomultiplier tube Part No H10330A-75). The quantum efficiency of the PMT at 1651 nm was approximately 1%. A high speed amplifier amplified the PMT signal for data acquisition. A computer with a field programmable gate array FPGA (National Instruments 7831-R), along with two delay generators (Stanford Research Systems DG645) provide the necessary timing signals, wavelength scan waveforms and appropriate delays for the data acquisition system. The major parameters of the airborne system are summarized in Table 1 below.

Table 1 Flight Lidar parameters

Parameter	Value
Seed Wavelength	1650.9 nm
Pump Wavelength	1064 nm
Laser Pulse Rate	~6.3 kHz
Laser Pulse Width	3 nsec
Laser Pump Energy	60 μJ
Seed Power	15 mW
OPA Energy	10 μJ
Laser Divergence	~300 μrad
Receiver Diameter	20 cm
Receiver Field of view	300 μrad
Receiver band pass	800 pm (FWHM)
Scan rate	~250 Hz
Averaging period	1 sec
Detector Efficiency	~1%

The lidar receiver electronics had to accommodate the various flight conditions (changing altitude and topography) and the photon counting detector input.

The flight data acquisition system used the PMT in analog mode. A gated integrator (Signal Recovery Model 4121B) integrated the return pulses and produced a time series of the transmittance through the atmospheric column. The seed wavelength was step-scanned over the absorption line using 20 evenly spaced wavelengths. The gate window for the return pulses was set to 20 ns and its delay was set by the FPGA. The delay was adjusted during flight by measuring the time of flight (TOF) between the start and the echo pulse. All the data was time tagged by a GPS unit that also provided position information.

5. Aircraft and Flights

The airborne flights were performed on NASA's DC-8 aircraft, which is based at the Dryden Airborne operations Facility (DAOF) in Palmdale, CA. Just prior to our methane flights the NASA ASCENDS program had completed a series of flights to measure column CO_2 using the same aircraft. We were able to share some of the GSFC personnel and equipment to minimize cost for these experiments. We chose to overfly the California Central Valley because of its proximity to Palmdale and for its possible methane sources (livestock feedlots, oil fields and natural gas storage sites). The flight instrument was integrated onto the airplane in early August 2011. The instrument complement included the GSFC CO_2 Sounder GPS, a Picarro in-situ analyzer that measures methane, carbon dioxide, and water vapor using Wavelength-Scanned Cavity Ring Down Spectroscopy (WS-CRDS) [32], and other ancillary instruments (Figure 4).

Figure 4 NASA's DC-8 aircraft at DAOF prior to a methane flight (left) and the methane lidar in the aircraft (right). The lidar used two aircraft racks and a transceiver.

The methane lidar flew three flights over California's Central Valley on August 23rd, 24th and 25th, 2011. All the flights traversed similar paths and were routed away from high traffic and adjacent military operations areas. The flight paths were anchored near Bakersfield, CA at the southern end and near Coalinga at the northern end. Each flight lasted about 2.5 hours and consisted of several segments at constant altitudes at approximately 3, 4.8, 6.2, 7.9, 9.5, and 11.1 km (10, 15, 20, 25, 30, 36 kft). The exact altitudes varied slightly with each flight. The flight paths and altitude profiles for the three flights are shown in Figure 5 and Figure 6 respectively. The order of the flight altitude segments was reversed for the August 25th flight and the flight

path deviated slightly to the west compared to the two previous flights. The terrain in the central valley varies between dry desert and cultivated areas with a gently changing topography.

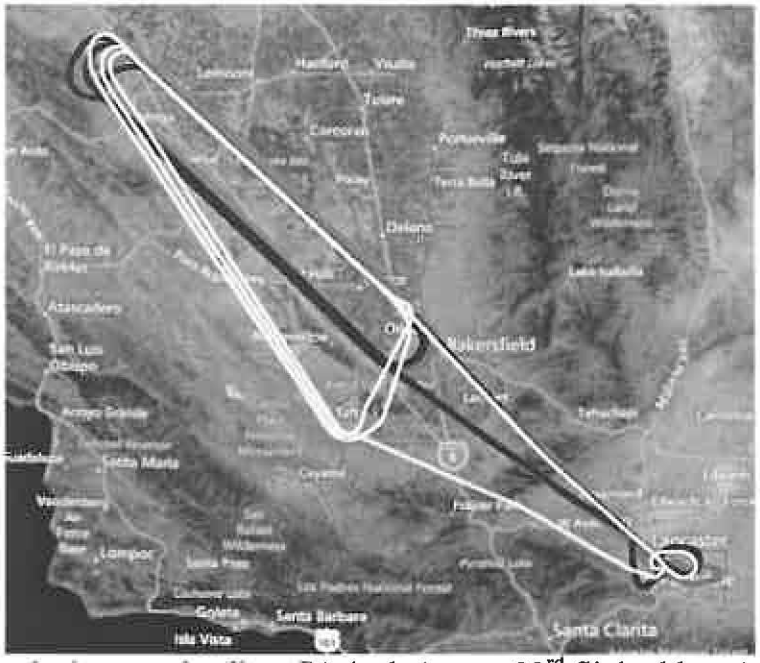

Figure 5 Flight paths in central valley, CA (red: August 23rd flight; blue: August 24th flight; yellow: August 25th flight)

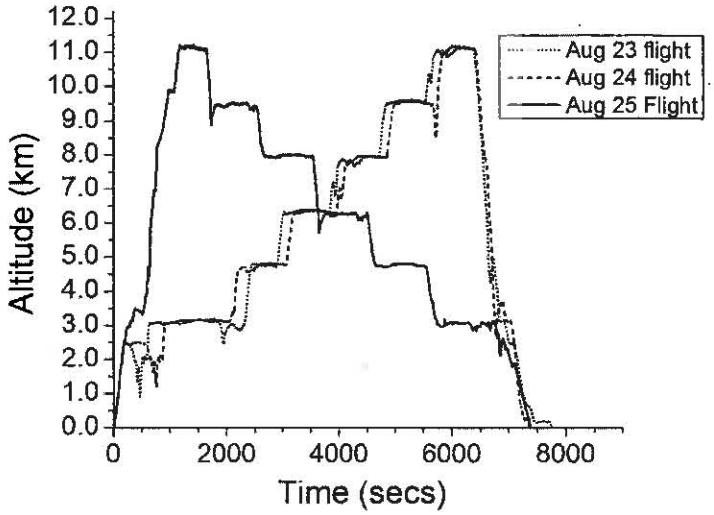

Figure 6 Flight altitude profiles for the three methane lidar flights in 2011

6. Airborne Measurements and Results

The integrated, normalized return pulse energies from the lidar as a function of wavelength represent the transmittance through the atmospheric column. Our retrieval algorithm

fits the transmittance or optical depth (OD) to the expected theoretical values in post-processing. The theoretical are generated by calculating the transmittance for each layer as a function of range, pressure, temperature, water vapor pressure and of course, the mixing ratio of methane and other atmospheric constituents. The calculations use line-by-line radiative transfer model [50] and the HITRAN 2008 data base. The range to the ground is determined by the time of flight between the start pulse and the echo pulse using the field programmable gate array (FPGA). The accuracy of the range measurement was approximately 2 m, comparable to what was obtained by Amediek et.al. [51] with a similar lidar instrument. Ancillary meteorological data is also needed to calculate the state of the atmosphere and implement a retrieval algorithm. Most of the additional meteorological data came from the aircraft data acquisition system which measures pressure, temperature, GPS location, dew point, wind speed, and many other parameters of interest. Our flight segments were relatively close to each other and the airplane meteorological data was adequate in providing data for the atmospheric layers above 3 km. However, we needed additional data for the layers below 3 km. The meteorological data during the ascend and descend to Palmdale were not useful since they were not taken in the vicinity of our main flight path. We obtained the additional meteorological data for our flights from the Global Modeling and Assimilation Office [52]. The GMAO develops models and assimilates observations from satellites and ground systems to generate meteorological products that are used for various NASA missions. Using these data we calculated the theoretical spectra of the expected atmospheric transmittance, OD, and Differential Optical Depth (DOD) as a function of altitude an example of which is illustrated in Figure 7.

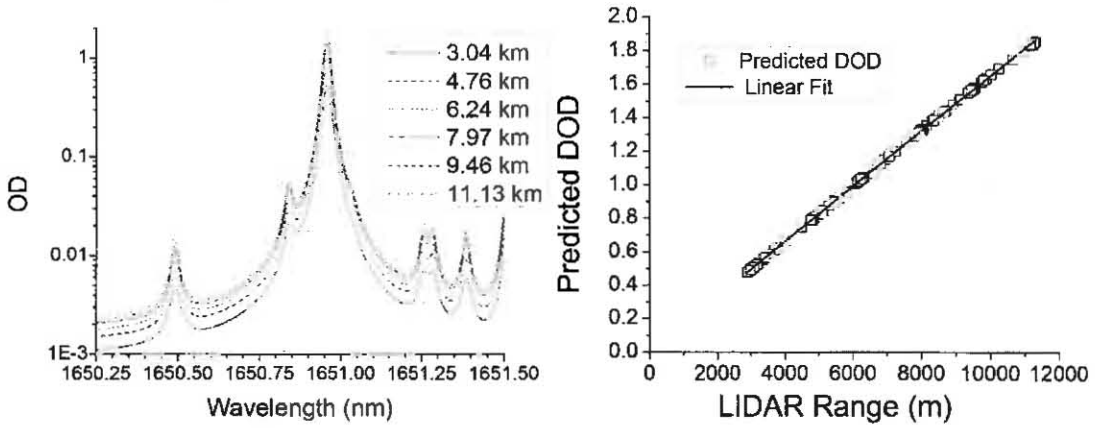

Figure 7 Examples of calculated Optical Depth (OD) examples (log scale) as a function of wavelength for different flight altitudes, and calculated Differential Optical Depth (DOD) as a function of altitude for the August 25th flight using GMAO data and HITRAN 2008.

An example of the measured transmittance vs. wavelength from 9.6 km altitude for the August 25th flight is shown in Figure 8. A 20 s averaging period was used and the baseline offset was removed. After the OD fit of the experimental to the theoretical data, the DOD is determined by subtracting the OD values at the "on" and "off" wavelengths. The on and off wavelengths are chosen from the 20 wavelengths used in the scan, typically the "on" being the peak of the line and "off" on the wing of the line. An on-board methane cell serves as a calibration for the wavelength scan across the absorption line.

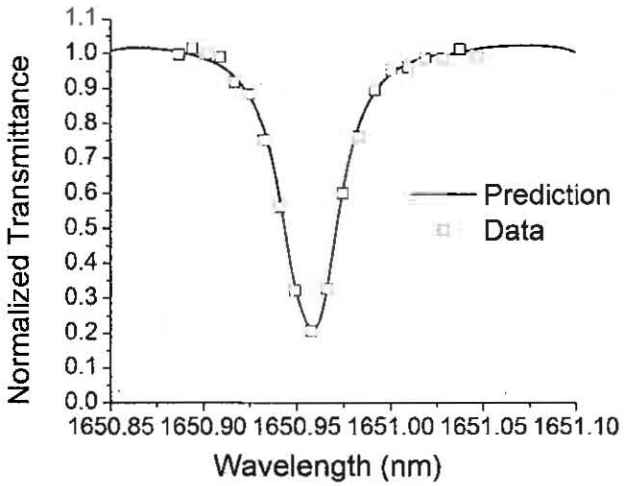

Figure 8 Retrieved transmittance vs. wavelength at a flight altitude of 9.6 km and comparison with the prediction using line by line calculations with the HITRAN 2008 database for the August 25th flight. A 20 sec averaging period was used.

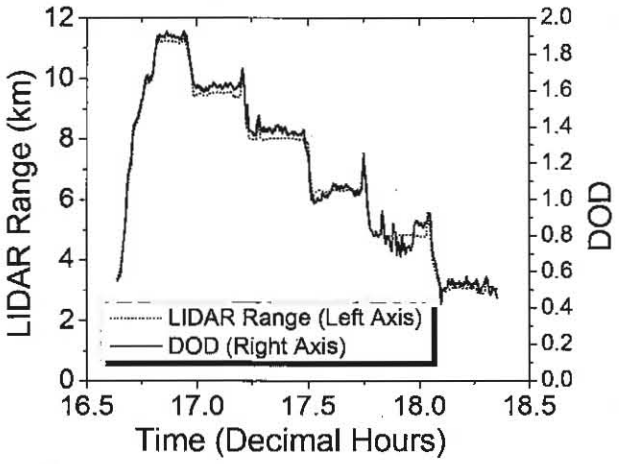

Figure 9 Measured lidar range and the corresponding DOD vs. time for the August 25th flight

Figure 9 shows the retrieved DOD as a function of altitude and compared to that calculated from theory. As expected the measured DOD increases with flight altitude. In addition, at each flight altitude change when the plane is turning the DOD increases because of the longer (slant) optical path. Figure 10 shows a comparison of the measured lidar DOD and the DOD predictions. A linear fit of the measured DOD vs. the theoretical DOD prediction shows a slope of 1.036 and a small offset of -0.012. The R^2 value of the fit is 0.994. The standard error in the slope estimate was 0.00045 and the standard deviation of the residuals of the fit was 0.0033.

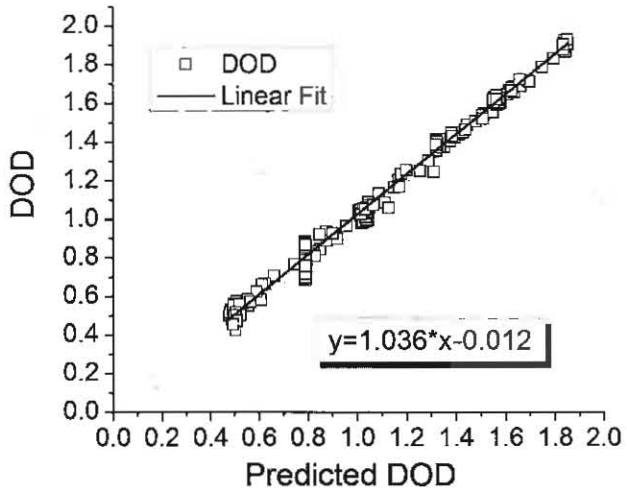

Figure 10Measured DOD vs. theoretical DOD prediction with a linear fit for the August 25th flight (right). A 20 s averaging period was used.

Along with the DOD, the retrievals estimated the methane column mixing ratio. Figure 11 shows the methane mixing ratio for the August 25th flight along with the in-situ CRDS instrument (Picarro) values as a function of flight time in decimal hours (UTC). A 20 s averaging period was used.

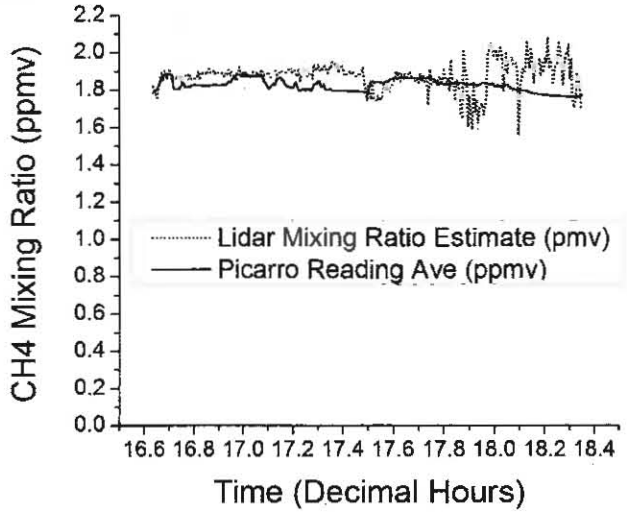

Figure 11 Comparison of the lidar methane mixing ratio with the in-situ CRDS instrument (Picarro) values as a function of flight time in decimal hours (UTC) for the August 25th flight. A 20 s averaging period was used.

7. Discussion

Overall the lidar and the Picarro showed good reasonable agreement. The lidar mixing ratio values were noisier and varied more than the Picarro. The noise increased at lower altitudes where the methane absorption gets smaller as the range (path length) gets shorter. Some of the sudden changes in the methane mixing ratio were due to alignment adjustments of the instrument during flight. We do not expect the lidar and the Picarro to agree perfectly. The in-situ

measurements are point measurements taken at a particular flight altitude whereas the methane lidar measures the entire column to the surface.

The lidar measurements were affected by several random and systematic noise sources. The low quantum efficiency of the PMT at 1651 nm and the relatively low power of the laser transmitter produced noisy data. The boresight alignment was also an issue and we had to check and adjust the receiver alignment during flight. This issue can be mitigated by a more robust opto-mechanical design. Finally one other significant non-random noise component that degraded our SNR was etalon fringes in our transmitter. Etalon fringes are unwanted optical interference patterns that arise from multiple weak reflections from each optical surface in the optical path. They are a function of small pathlength changes due to opto-mechnical shifts, temperature, and changes in the index of refraction and they can limit the detection sensitivity and averaging time of a laser spectrometer [53]. Various signal processing techniques have been suggested for reducing their impact [54-56] but none of these techniques have been completely successful. Our transmitted beam exhibited a large fringe which was then superimposed on the return pulses. We believe that the fringe is the result of reflections from the crystal or one of the other optical elements in the path (lenses and beam splitters). On the ground system we were able to use the energy monitor signal to remove the effect of the etalon fringe. Unfortunately on the flight system the normalization with the energy monitor actually proved detrimental since the fringes on the receiver and the energy monitor exhibited different phases and free spectral range. The presence of the fringe limited the ability of the fitting algorithm to find a good fit and increased our overall error. We believe that with better opto-mechanical design and adequate pre-flight testing we can overcome these problems and improve our results.

8. Summary

We have demonstrated airborne measurements of methane absorption and column abundance using a pulsed direct detection lidar and the IPDA technique. The lidar operates at the 1650.95 nm methane line and the laser was stepped-scanned over the absorption with 20 evenly spaced wavelength steps. The return pulses are gated and integrated to produce a transmittance measurement through the atmospheric column. We flew three flights in the central valley of CA on NASA's DC-8 flying laboratory. All flights consisted of flight segments at stepped altitudes from 3 to11 km. A retrieval algorithm estimated the optical depth and methane mixing ratio by fitting the experimental data to the theoretical predictions. The fitted line shapes agreed well with those predicted from the line-by-line radiative transfer calculations with the HITRAN 2008 database and the airplane and GMAO meteorological data.

The dominant error source for these flights was etalon fringes in the lidar that added unwanted structure to our line shapes. The low transmitter power and 1% quantum efficiency of the detector and were also significant limitations. We are currently in the process of increasing the power of the laser transmitter and the detector sensitivity. With improved stability, higher laser power and detector efficiency this approach can be used for airborne studies of methane column for carbon cycle science investigations. Once further laser power scaling and detector improvements are accomplished a space lidar using this approach should be feasible.

Acknowledgments

This research was funded by the NASA Astrobiology Technology Instrument Development program. We would like to thank Dr. Michael New for his support throughout the program. We would also like to thank the Earth Science Technology Office (ESTO), and the Instrument

Incubation Program, and the Goddard CO_2 Sounder team for their equipment loan and for their assistance.

1. Intergovernmental Panel on Climate Change Report (IPCC), 2007, Available at: http://www.ipcc.ch/index.htm
2. P. Bergamaschi, Frankenberg, C., Meirink, J.F., Krol, M.C., Dentener, F.J.; Wagner, T., Platt, U., Kaplan, J.O., Körner, S.; Heimann, M.; Dlugokencky, E.J.; Goede, A. De, "Satellite chartography of atmospheric methane from SCIAMACHY on board ENVISAT2. Evaluation based on inverse model simulations", Journal of Geophysical Research-Atmospheres, Volume: 112 (2007), pp. D02304/1-D02304/26
3. M. Buchwitz, R. De Beek, J. P. Burrows, H. Bovensmann, T. Warneke, J. Notholt, J. F. Meirink, A. P. H. Goede , P. Bergamaschi, S. Körner, M. Heimann, A. Schulz, "Atmospheric methane and carbon dioxide from SCIAMACHY satellite data: initial comparison with chemistry and transport models", Atmos. Chem. Phys., 5, 941–962, 2005
4. C. Frankenberg, J. F. Meirink, P. Bergamaschi, A. P. H. Goede, M. Heimann, S. Körner, U. Platt, M. van Weele, T. Wagner, " Satellite cartography of atmospheric methane from SCIAMACHY on board ENVISAT: Analysis of the years 2003 and 2004", Journal of Geophysical Research, Vol. 111, D07303, 2006 doi:10.1029/2005JD006235
5. A. Razavi, Clerbaux, C., Wespes, C., Clarisse, L., Hurtmans, D., Payan, S., Camy-Peyret, C., and Coheur, P., "Characterization of methane retrievals from the IASI space-borne sounder", Atmos. Chem. Phys., 9, 7889–7899, 2009.
6. T. August, Klaes, D., Schlussel, P., Hultberg, T., Crapeau, M., Arriaga, A., O'Carroll, A., Coppens, D., Munro, R., Calbet, X., "IASI onMetop-A: Operational Level 2 retrievals after five years in orbit", Journal of Quantitative Spectroscopy & Radiative Transfer 113 (2012), 1340–1371.
7. P. F. Coheur, Xiong, X., C. D. Barnet, Q. Zhuang, T. Machida, C. Sweeney, and P. K. Patra (2010), Mid-upper tropospheric methane in the high Northern Hemisphere: Spaceborne observations by AIRS, aircraft measurements, and model simulations, J. Geophys. Res., 115, D19309, doi:10.1029/2009JD013796
8. X. Xiong, Barnet C., Maddy E., Wei J., Liu X., Pagano T.S. Seven Years' Observation of Mid-Upper Tropospheric Methane from Atmospheric Infrared Sounder. Remote Sensing. 2010; 2(11): 2509-2530.
9. T. Yokota, Oguma, H., Morino, I., Higurashi, A., Aoki, T. et. al. "Test measurements by a BBM of the nadir-looking SWIR FTS aboard GOSAT to monitor CO2 column density from Space". Proc. SPIE. 2004, 5652, 182, doi:10.1117/12.578497.
10. T. Yokota, Y. Yoshida, N. Eguchi, Y. Ota, T. Tanaka, H. Watanabe, and S. Maksyutov, "Global Concentrations of CO2 and CH4 Retrieved from GOSAT: First Preliminary Results", SOLA, 2009, Vol. 5, 160–163, doi:10.2151/sola.2009–041
11. I. Morino, O. Uchino, M. Inoue, Y. Yoshida, T. Yokota, P. O. Wennberg, G. C. Toon, D. Wunch, C. M. Roehl, J. Notholt, T. Warneke, J. Messerschmidt, D. W. T. Griffith, N. M. Deutscher, V. Sherlock, B. Connor, J. Robinson, R. Sussmann, and M. Rettinger,

"Preliminary validation of column-averaged volume mixing ratios of carbon dioxide and methane retrieved from GOSAT short-wavelength infrared spectra," Atmos. Meas. Tech., 4, 1061–1076, 2011, doi:10.5194/amt-4-1061-2011

12. Y. Yoshida, Ota Yoshifumi, Eguchi Nawo, Kikuchi Nobuhiro, Nobuta Koji, Tran Ha, Morino Isamu, Yokota Tatsuya: Retrieval algorithm for CO2 and CH4 column abundances from short-wavelength infrared spectral observations by the Greenhouse Gases Observing Satellite, Atmos. Meas. Tech., 4, 717-734, doi:10.5194/amt-4-717-2011, 2011.
13. J. Mao, and S. R. Kawa, "Sensitivity studies for space-based measurement of atmospheric total column carbon dioxide by reflected sunlight," Applied Optics, 43, 914-927, 2004.
14. I. Aben, O. Hasekamp, and W. Hartmann, Uncertainties in the space-based measurements Of CO2 columns due to scattering in the Earth's atmosphere, J. Quant. Spectrosc. Radiat. Transfer, 104, 450-459, 2007.
15. E. S. Maddy, C. D. Barnet, M. Goldberg, C. Sweeney, and X. Liu, CO2 retrievals from the Atmospheric Infrared Sounder: Methodology and validation, J. Geophys. Res., 113, D11301, doi:10.1029/2007JD009402, 2008.
16. E.J. Dlugokencky, et al., "Atmospheric methane levels off: Temporary pause or a new steady state". Geophys. Res. Lett., 30, 2003, doi:10.1029/2003GL018126
17. E. J. Dlugokencky, et al. (2009), Observational constraints on recent increases in the atmospheric CH4 burden, Geophys. Res. Lett., 36, L18803, doi:10.1029/2009GL039780.
18. K. Kvenvolden, "Methanehydrate - A major reservoir of carbon in the shallow geosphere?", Chemical Geology, Vol. 71, 41–51, (1988).
19. F. Keppler, Hamilton J.T.G., Bra M., Roeckmann T., "Methane emissions from terrestrial plants under aerobic conditions", Nature 439, 187-191, 2006.
20. T.R. Christensen, et al., 2004, "Thawing sub-arctic permafrost: Effects on vegetation and methane emissions". Geophys. Res. Lett., 31, doi:10.1029/2003GL018680
21. W. Anthony, K. Anthony, P., Grosse, G., and Chanton, J., "Geologic methane seeps along boundaries of Arctic permafrost thaw and melting glaciers", Nature Geoscience 5, 419–426, (2012), doi:10.1038/ngeo1480.
22. E. Kort, Wofsy, S., Daube, B., Diao, Elkins, J., Gao, R., Hintsa, E., Hurst, D., Jimenez, R., Moore, F., Spackman, J., Zondio, M., "Atmospheric Observations of Arctic Ocean methane emissions up to 82o north", Nature Geoscience 5, 318–321 (2012), doi:10.1038/ngeo1452.
23. J. Houghton, et al., Eds., Climate Change 2001: The Scientific Basis, Cambridge Univ. Press, Cambridge, 2001.
24. National Research Council Decadal Survey: Earth Science and Applications from Space: National Imperatives for the Next Decade and Beyond, National Academic Press, 2007

25. NASA ASCENDS Workshop at http://cce.nasa.gov/ascends/index.htm
26. G. Ehret, Fix, A., Kiemle, C., and Wirth, A., " Space-borne monitoring of methane by intergrated parth differential absorption lidar: Perspective of DLR`s CHARM-SSB mission", Proc. 24th International Laser Radar Conference, pp. 1208-1211, 2008.
27. C. Stephan, M. Alpers; B. Millet; G. Ehret; P. Flamant; C. Deniel, "MERLIN: a space-based methane monitor", "Lidar Remote Sensing for Environmental Monitoring XII. Proceedings of the SPIE, Volume 8159, pp. 815908-815908-15 (2011).
28. A. Fix, Christian Büdenbender; Martin Wirth; Mathieu Quatrevalet; Axel Amediek; Christoph Kiemle; Gerhard Ehret, "Optical parametric oscillators and amplifiers for airborne and spaceborne active remote sensing of CO2 and CH4 Lidar Technologies", Techniques, and Measurements for Atmospheric Remote Sensing VII. Proceedings of the SPIE, Volume 8182, pp. 818206-818206-10 (2011)
29. M.D. Smith, "Spacecraft observations of the Martian atmosphere", Annu. Rev. Earth Planet. Sci., 36: 191-219, 2008.
30. M.J. Mumma, R.E. Novak, M.A. DiSanti and B.P. Bonev, "A sensitive search for methane on Mars". AAS/Division for Planetary Sciences Meeting 35, 937–938, 2003.
31. M.J. Mumma, Novak RE, DiSanti MA, Bonev BP, Dello Russo N., "Detection and mapping of methane and water on Mars", Bull. Am. Astron. Soc. 36:1127, 2004
32. M.J. Mumma, Villanueva, G.L., Novak, Robert E., Hewagama, T. Bonev, B. P. et.al., " Strong Release of Methane on Mars in Northern Summer 2003", Science, Vol. 323. no. 5917, pp. 1041 – 1045, 2009, DOI: 10.1126/science.1165243
33. P.H. Smith, et.al. "H2O at the Phoenix Landing Site", Science 325, 58, 2009.
34. R. W. Zureka, Augustin Chicarrob, Mark A. Allen, Jean-Loup Bertaux, R.Todd Clancy, Frank Daerden, Vittorio Formisano, James B. Garvin, Gerhard Neukum, Michael D. Smith, "Assessment of a 2016 mission concept: The search for trace gases in the atmosphere of Mars", Planetary and Space Science Volume 59, Issues 2–3, February 2011, Pages 284–291.
35. K., Numata, Haris Riris, Steve Li, Stewart Wu, Stephan R. Kawa, Michael Krainak, James Abshire, "Ground demonstration of a trace gas lidar based on optical parametric amplifiers", accepted for publication to Applied Remote Sensing
36. H. Riris, Li, S.; Numata, K.; Wu, S.; Burris, J.; Yu, A. W.; Krainak, M.; Abshire, J. B. "Methane Measurements using Optical Parametric Technology", American Geophysical Union, Fall Meeting 2009, abstract #A41C-0106
37. D. G. Murdock, Stearns, S. V., Lines, R.T., Lenz, D., Brown, D.M., Philbrick, C.R., "Applications of real-world gas detection: Airborne Natural Gas Emission Lidar (ANGEL) system", Journal of Applied Remote Sensing, Vol. 2, 023518, May 2008.
38. A. Minato, Joarder, M.A., Ozawa, S., Kadoya, M., and Sugimoto, N., "Laser long-path absorption lidar technique for measuring methane using gas correlation method", Jpn. J. Appl. Phys. 38 (1999) pp. 6130-6132, 1999.

39. Y. Kamali, Daigle, J.F, Théberge, F., Châteauneuf, M., Azarm, A., et.al., "Remote sensing of trace methane using mobile femtosecond laser system of T&T Lab", Optics Communications 282, 2062–2065, 2009.
40. M.J.T. Milton, Gardiner, T.D., Molero, T., Galech, J., Injection-seeded optical parametric oscillator for range-resolved DIAL measurements of atmospheric methane, Optics Communications 142 (1997) 153-160, 1997.
41. E.R. Crosson, "A cavity ring-down analyzer for measuring atmospheric levels of methane, carbon dioxide, and water vapour", Applied Physics B 92, 3, pp. 403-408, 2008
42. C. Webster, "Measuring methane and its isotopes $^{12}CH4$, $^{13}CH4$, and CH3D on the surface of Mars with in situ laser spectroscopy", Applied Optics, Vol. 44, Issue 7, pp. 1226-1235 (2005)
43. S. Wright, G. Duxbury and N. Langford "A compact quantum-cascade laser based spectrometer for monitoring the concentrations of methane and nitrous oxide in the troposphere", Applied Physics B: Lasers and Optics, Volume 85, Numbers 2-3 (2006), 243-249, DOI: 10.1007/s00340-006-2384-x
44. L.S. Rothman, Gordon, I.E, Barbe, A., et.al. "The HITRAN 2008 molecular spectroscopic database", Journal of Quantitative Spectroscopy& Radiative Transfer110 (2009) 533–572, 2009
45. K. Numata, Chen, J.R., Wu, S.T., Abshire, J.B, and Krainak, M.A., " Frequency stabilization of distributed-feedback laser diodes at 1572 nm for lidar measurements of atmospheric carbon dioxide", Applied Optics, Vol. 50, No. 7, 1047, 2011.
46. A. Amediek, Fix, A., Wirth, M., Ehret, G., "Development of an OPO system at 1.57 μm for integrated path DIAL measurement of atmospheric carbon dioxide", Appl. Phys. B 92, 295–302 (2008), DOI: 10.1007/s00340-008-3075-6.
47. R. Measures, *Laser Remote Sensing*, John Wiley & Sons, New York, 1984
48. J.B. Abshire, Riris. H., Allan, G., Weaver C.J., Mao, J. Xiaoli Sun, X., Hasselbrack, W.E., Kawa, R.S, and Biraud, S., "Pulsed airborne lidar measurements of atmospheric CO2 column absorption", Tellus, 62B, 770–783, 2010.
49. G. Ehret, Kiemel, C., Wirth W., Amediek, A., et.al., "Space-borne remote sensing of CO2, CH4, and N2O by integrated path differential absorption lidar: a sensitivity analysis", Appl. Phys. B 90, 593–608, 2008.
50. S.A. Clough and M.J. Iacono, "Line-by-line calculations of atmospheric fluxes and cooling rates. 2: Applications to carbon dioxide, ozone, methane, nitrous oxide, and the halocarbons," J. of Geophys. Res. 100,16519-16535, 1995.
51. A. Amediek, X. Sun, and J. B. Abshire, "Analysis of Column Height Measurements from a Pulsed Airborne CO2 Integrated Path Differential Absorption Lidar", submitted for publication to Transactions on Geoscience and Remote Sensing.
52. Global Modeling and Assimilation Office available at http://gmao.gsfc.nasa.gov/

53. P. Werle, R. Mucke, F. Slemr, "The Limits of Signal Averaging in Atmospheric Trace-Gas Monitoring by Tunable Diode-Laser Absorption Spectroscopy (TDLAS)", Appl. Phys. B 57, 131-139, 1993.
54. P. Werle, P. Mazzinghi, F. D'Amato, M. De Rosa, K. Maurer, F. Slemr, "Signal processing and calibration procedures for in situ diode-laser absorption spectroscopy", Spectrochimica Acta Part A 60,1685–1705, 2004.
55. H. Riris, C. B. Carlisle, R.E. Warren, D. E. Cooper, Signal to Noise Ratio Enhancement in Frequency Modulation Spectrometers Using Digital Signal Processing, Opt. Let., 32, 144, 1994.
56. D.S. Bomse, and D.J. Kane, "An adaptive singular value decomposition (SVD) algorithm for analysis of wavelength modulation spectra", Appl. Phys. B 85, 461–466, (2006).